Supplementary material

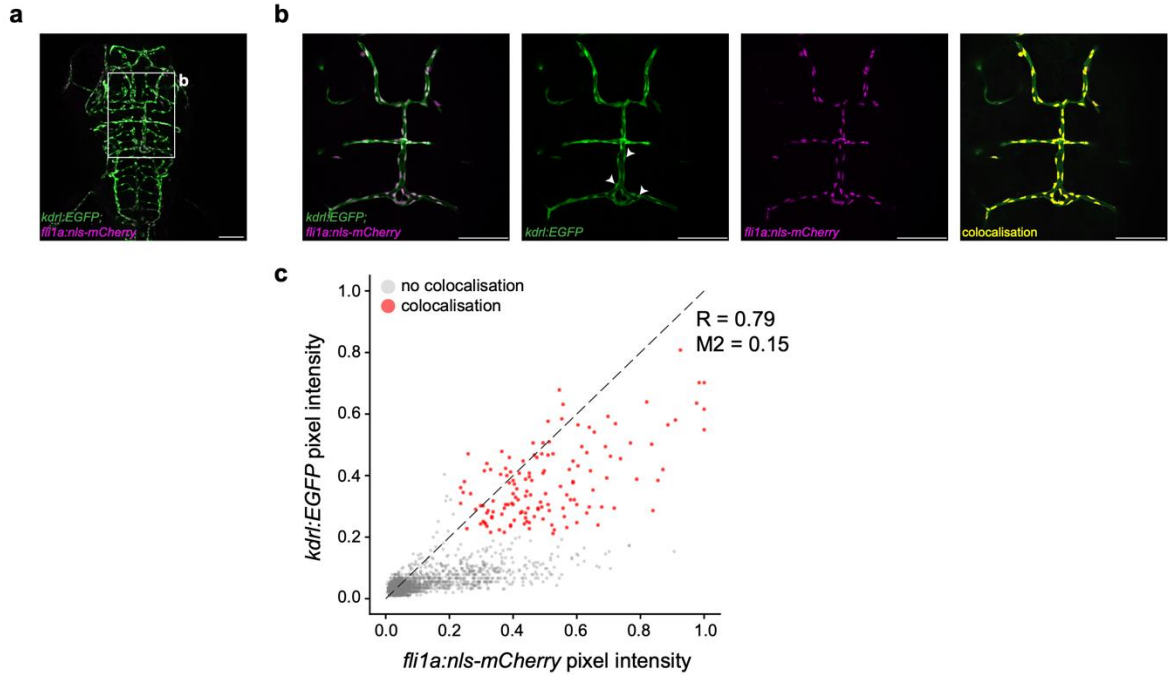

Fig. S1. *Tg(kdrl:EGFP)^{s843}* presents perinuclear EGFP within the zebrafish vasculature. **a**) Representative confocal image displaying brain vasculature of *Tg(kdrl:EGFP)^{s843};Tg(fli1a:nls-mCherry)^{sh550}* zebrafish embryo at 3 dpf. **b**) Enlarged views from (**a**) are displayed: overlay image (first), *Tg(kdrl:EGFP)^{s843}* channel (second), *Tg(fli1a:nls-mCherry)^{sh550}* channel (third), and co-localisation mask (fourth). **c**) Correlation plot of *kdrl:EGFP* and *fli1a:nls-mCherry* pixel intensities. Pearson correlation coefficient (R) and Manders' coefficient (M2) are indicated. Scale bars = 100μm.

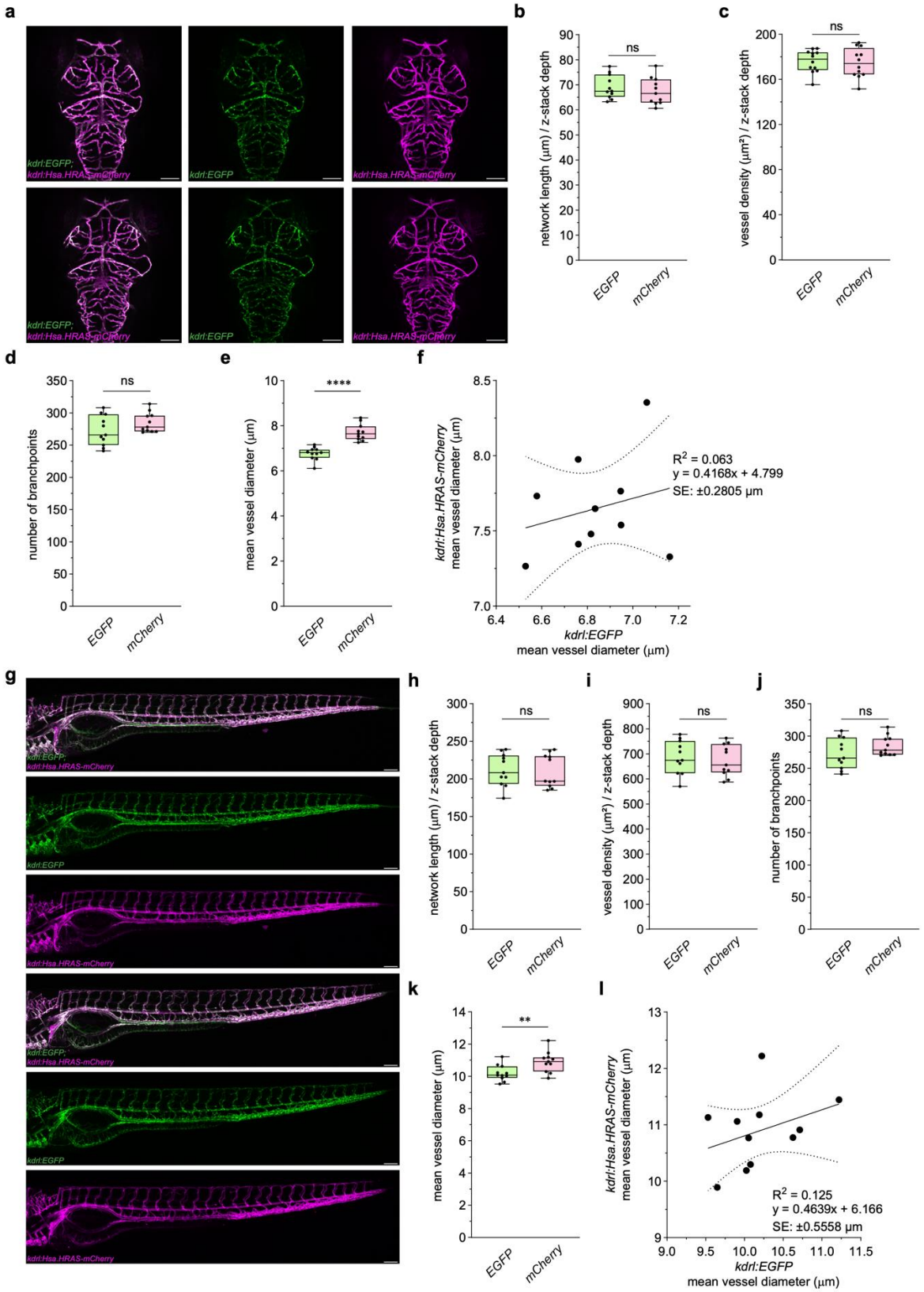

Fig. S2. VISTA-Z captures complex vascular and reveals transgene-mediated differences in vessel diameter. a) Two representative confocal images of the brain vasculature of zebrafish embryos at 5 dpf. Overlay of *Tg(kdrl:EGFP)*^{s843};*Tg(kdrl:Hsa.HRAS-mCherry)*^{s916} (left) or individual channels (right). **b - e**) Quantification of vascular metrics including normalised network length (**b**, ns = 0.4147), vessel density (**c**, ns = 0.3173), number of branchpoints (**d**, ns =

0.1816), and vessel diameter (**e,** p ≤ 0.0001). **f**) Correlation analyses compare vessel diameters measured in *Tg(kdrl:EGFP)*^{s843} or *Tg(kdrl:Hsa.HRAS-mCherry)*^{s916}. The equation of the regression line, R-squared (R^2) and standard error (SE) are represented in the graph. **g**) Two representative confocal images show the trunk vasculature of zebrafish embryos at 5 dpf. Overlay of *Tg(kdrl:EGFP)*^{s843};*Tg(kdrl:Hsa.HRAS-mCherry)*^{s916} (top) or individual channels (bottom). **h - k**) Quantification of vascular metrics including normalised network length (**h**, ns = 0.3203), vessel density (**i**, ns = 0.1887), number of branchpoints (**j**, ns = 0.2105), and vessel diameter (**k,** p = 0.0055). **l**) Correlation analyses of vessel diameters as described in (**f**). All panels represent n = 11 embryos, except for n = 10 embryos (**f**) obtained from two independent breeding pairs. Statistical significance was assessed using paired Student's t-test for all panels, except for panel (**h**), which used Wilcoxon test. Scale bars = 100μm.

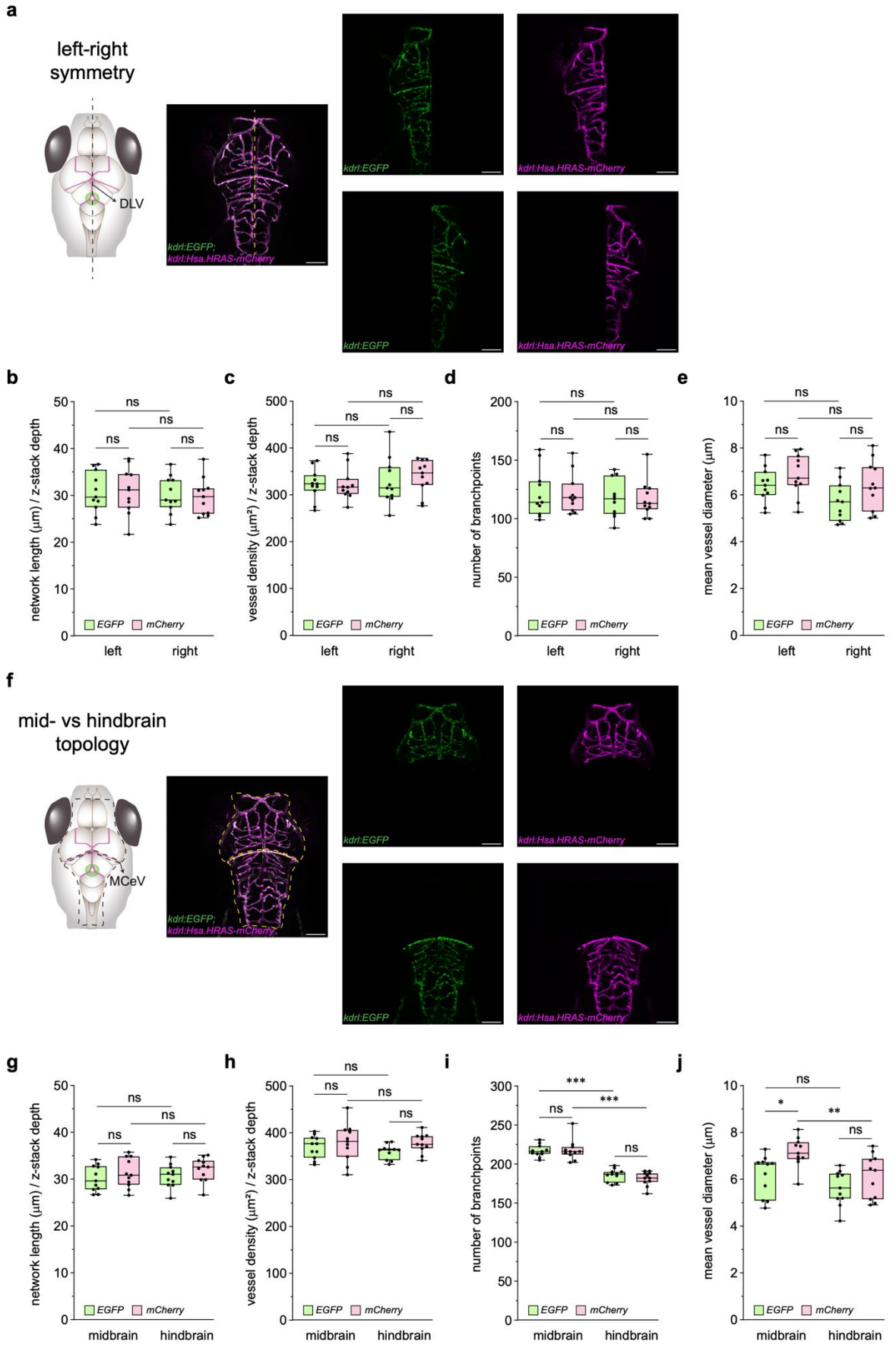

Fig. S3. VISTA-Z enables ROI-based regional vascular analysis. a) Representative diagram (left) and confocal images (right) of the brain vasculature at

3 dpf showing left-right symmetry in *Tg(kdrl:EGFP)^{s843}*;*Tg(kdrl:Hsa.HRAS-mCherry)^{s916}* embryos. Overlay (left) and individual channels (right) are displayed. **b - e**) Quantification of vascular metrics for left and right regions, including normalised network length (**b**, ns = 0.9988 (left), ns = 0.9914 (right), ns = 0.9078 (mCherry) and ns = 0.9956 (EGFP)), vessel density (**c**, ns > 0.9999 (left), ns = 0.9132 (right), ns = 0.7023 (mCherry) and ns = 0.9814 (EGFP)), number of branchpoints (**d**, ns = 0.8561 (left), ns = 0.8561 (right), ns = 0.2860 (mCherry) and ns = 0.5128 (EGFP)), and vessel diameter (**e**, ns = 0.6610 (left), ns = 0.2549 (right), ns = 0.6543 (mCherry) and ns = 0.2502 (EGFP)). **f**) Representative diagram (left) and confocal images (right) of brain vasculature at 3 dpf showing midbrain versus hindbrain vasculature in *Tg(kdrl:EGFP)^{s843}*;*Tg(kdrl:Hsa.HRAS-mCherry)^{s916}* embryos. Overlay and individual channels are displayed as in (**a**). **g - j**) Quantification of vascular metrics for midbrain and hindbrain regions, including normalised network length (**g**, ns = 0.7616 (midbrain), ns = 0.6267 (hindbrain), ns = 0.9064 (mCherry) and ns = 0.9697 (EGFP)), vessel density (**h**, ns = 0.8607 (midbrain), ns = 0.3867 (hindbrain), ns = 0.9998 (mCherry) and ns = 0.8017 (EGFP)), number of branchpoints (**i**, ns = 0.7891 (midbrain), ns = 0.0986 (hindbrain), p = 0.001 (mCherry) and p = 0.001 (EGFP)), and vessel diameter (**j**, p = 0.0278 (midbrain), ns = 0.5114 (hindbrain), p = 0.0182 (mCherry) and ns = 0.4129 (EGFP)). All panels represent n = 11 embryos from two independent breeding pairs. Statistical significance was assessed using two-way ANOVA with Tukey's multiple comparisons correction, except for panels (**d** and **i**), which used Kruskal-Wallis test with false discovery rate correction. Scale bars = 100μm.

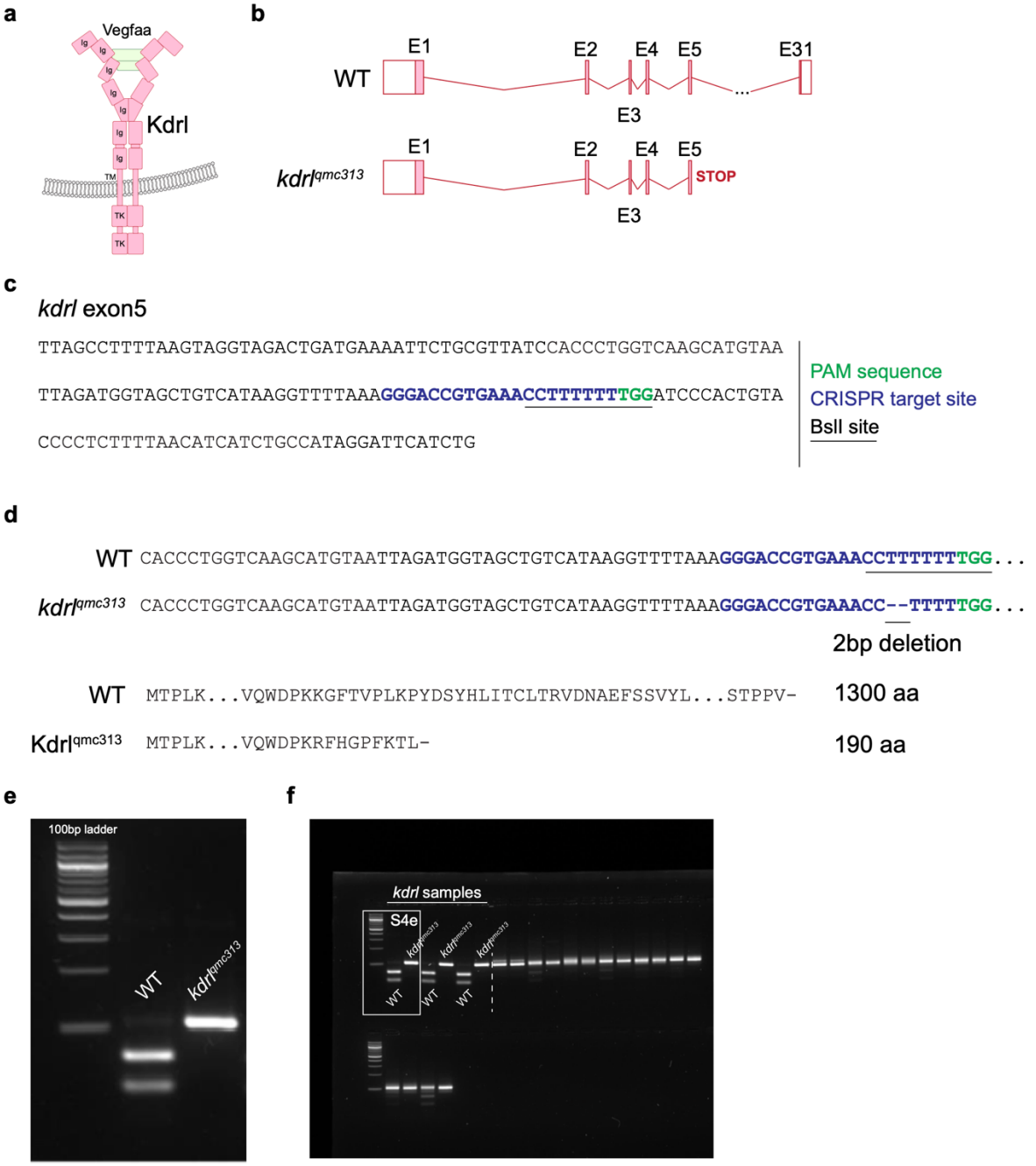

Fig. S4. Characterisation of *kdrl*^{qmc313} mutant allele. **a**) Schematic representation of the Kdrl domains, including seven tandem immunoglobulin-like (Ig) domains, transmembrane (TM) region, and tyrosine kinase (TK) domains. Kdrl ligand Vegfaa is represented within the pocket site. **b**) Diagram of wild type *kdrl* (top) or *kdrl*^{qmc313} mutant (bottom) gene structures. The first exons are shown as (E1 – E5). Wild type kdrl sequence is represented with the last exon (E31), whereas the *kdrl*^{qmc313} allele is represented as a mutation within exon 5, resulting in a predictive premature stop codon. **c**) Sequence of wild type *kdrl* exon 5 highlighting the CRISPR target site (blue), PAM sequence (green), and BslI restriction site (underlined). **d**) Top: DNA sequence alignment of wild type and *kdrl*^{qmc313} mutant exon 5, colour-coded as described in (**c**). The 2bp deletion in the mutant allele is indicated with two dashes. Bottom: protein sequences for wild type and Kdrl^{qmc313} mutant. The latter shows the mutant protein truncates prematurely within the first 190 amino acids. aa: amino acids. **e**) Representative cropped gel electrophoresis image showing the presence

of a wild type amplicon (left) or the *kdrl*^{qmc313} mutant allele (right) after PCR amplification and BslI digestion. **f**) Uncropped agarose gel image corresponding to panel (**e**). The section shown in panel (**e**) is highlighted for reference. The gel includes three sets of samples, each containing one wild type amplicon (left) or the *kdrl*^{qmc313} mutant allele (right). Additional lanes present in the gel after the dotted line are unrelated to this experiment.

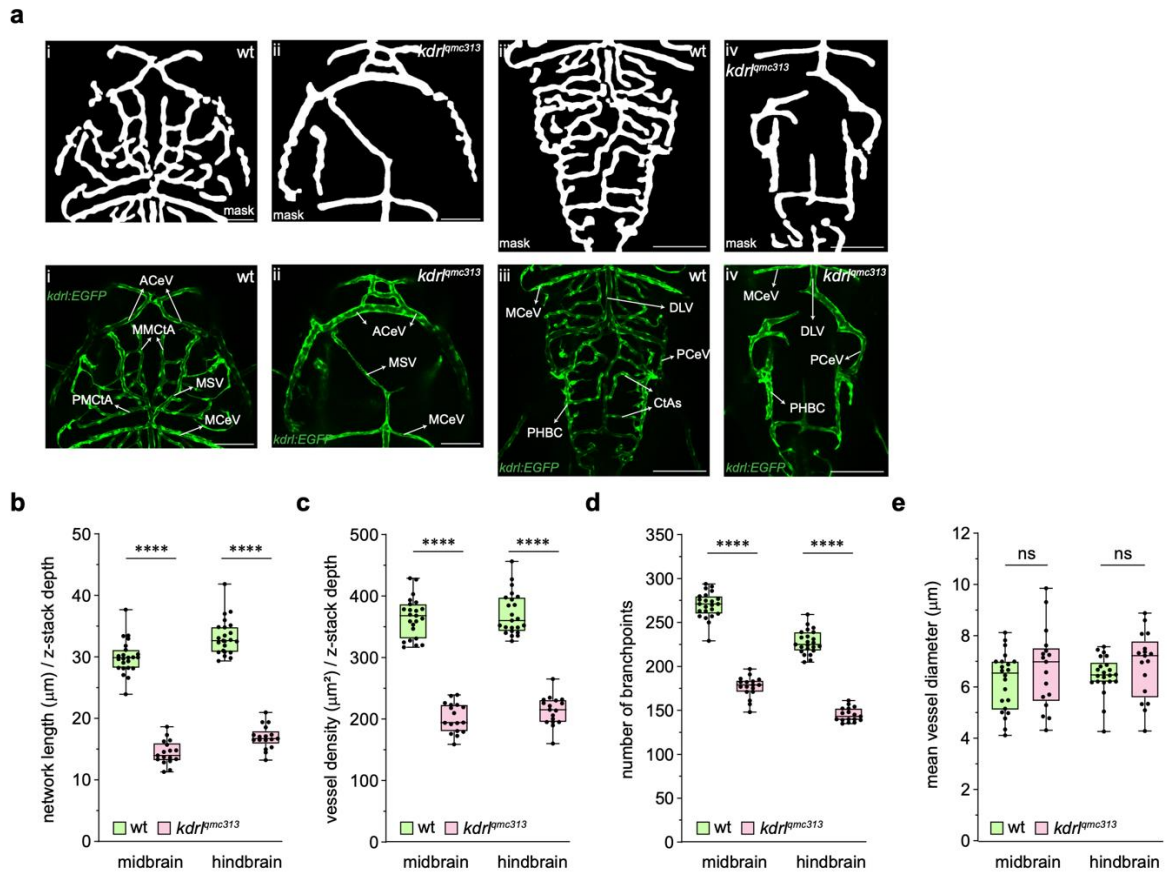

Fig. S5. VISTA-Z detects midbrain and hindbrain vascular defects in *kdrl* mutant embryos. a) Enlarged views of the brain vasculature from (**Fig. 5a**) showing midbrain (i and ii) and hindbrain (iii and iv) regions from wild type (left) and *kdrl* mutant (right) embryos at 3 dpf. Vessel segmentation masks (top) and confocal images (bottom). **b - e**) Quantification of vascular metrics in midbrain and hindbrain segments, including normalised network length (**b**, $p \leq 0.0001$ (midbrain) and $p \leq 0.0001$ (hindbrain)), vessel density (**c**, $p \leq 0.0001$ (midbrain) and $p \leq 0.0001$ (hindbrain)), number of branchpoints (**d**, $p \leq 0.0001$ (midbrain) and $p \leq 0.0001$ (hindbrain)), and vessel diameter (**e**, ns = 0.2442 (midbrain) and ns = 0.1308 (hindbrain)). All panels represent n = 23 wild type and n = 17 mutant embryos. Embryos were obtained from two independent breeding pairs. Statistical significance was assessed using unpaired Student's t-test for all panels, except for panels (**b**, **c** and **e**: hindbrain), which used Mann–Whitney U test. ACeV: anterior cerebral vein, CtAs: central arteries, DLV: dorsal longitudinal vein, MCeV: middle cerebral vein, MSV: mesencephalic vein, PCeV: posterior cerebral vein, PHBC: primordial hindbrain channels and PMCtA and MMCtA: posterior and middle mesencephalic central arteries. Scale bars = 100μm.

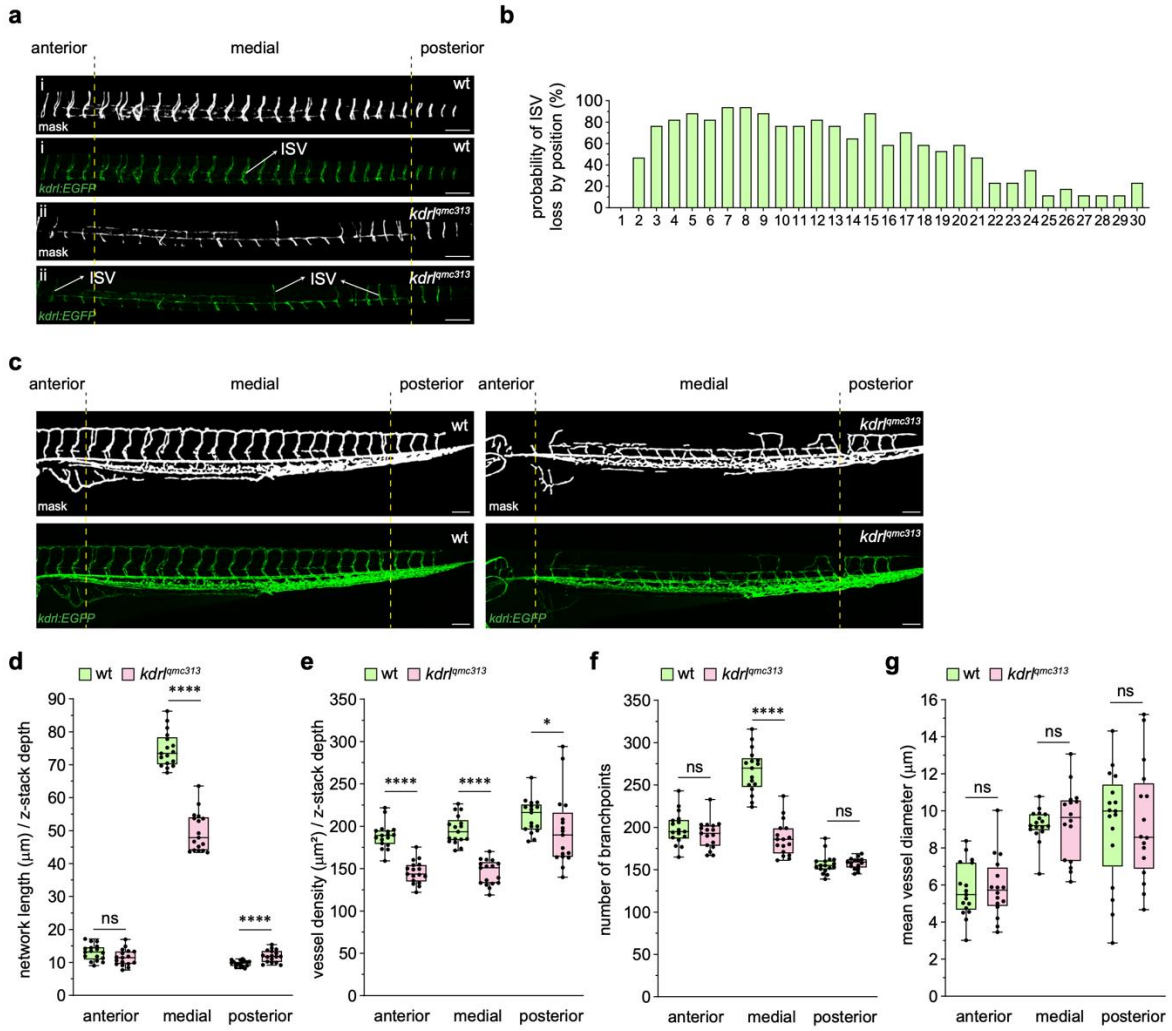

Fig. S6. VISTA-Z reveals regional differences in trunk vascular defects in *kdrl* mutant embryos. **a**) Vessel segmentation masks (top) and confocal images (bottom) of trunk ISVs from wild type (first and second) and *kdrl* mutant (third and fourth) embryos at 3 dpf. Regiones were defined as: anterior (ISVs 1-4), medial (ISVs 5-25), and posterior (ISVs 26-30). **b**) Probability of ISV loss by position. **c**) Vessel segmentation masks (top) and confocal images (bottom) of the trunk vasculature from wild type (left) and *kdrl* mutant (right) embryos. Regiones were defined as in (**a**). **d - g**) Quantification of vascular metrics in anterior, medial and posterior segments, including normalised network length (**d**, ns = 0.0739 (anterior), $p \leq 0.0001$ (medial) and $p \leq 0.0001$ (posterior)), vessel density (**e**, $p \leq 0.0001$ (anterior), $p \leq 0.0001$ (medial) and $p = 0.0447$ (posterior)), number of branchpoints (**f**, ns = 0.2535 (anterior), $p \leq 0.0001$ (medial) and ns = 0.2774 (posterior)), and vessel diameter (**g**, ns = 0.8107 (anterior), ns = 0.4654 (medial) and ns = 0.9451 (posterior)). All panels represent n = 17 embryos. Embryos were obtained from two independent breeding pairs. Statistical significance was assessed using unpaired Student's t-test for all panels, except for panels (**d**: medial, **g**: medial, **e**: posterior and **f**: posterior), which used Mann–Whitney U test. ISV: intersegmental vessel. Scale bars = 100µm.

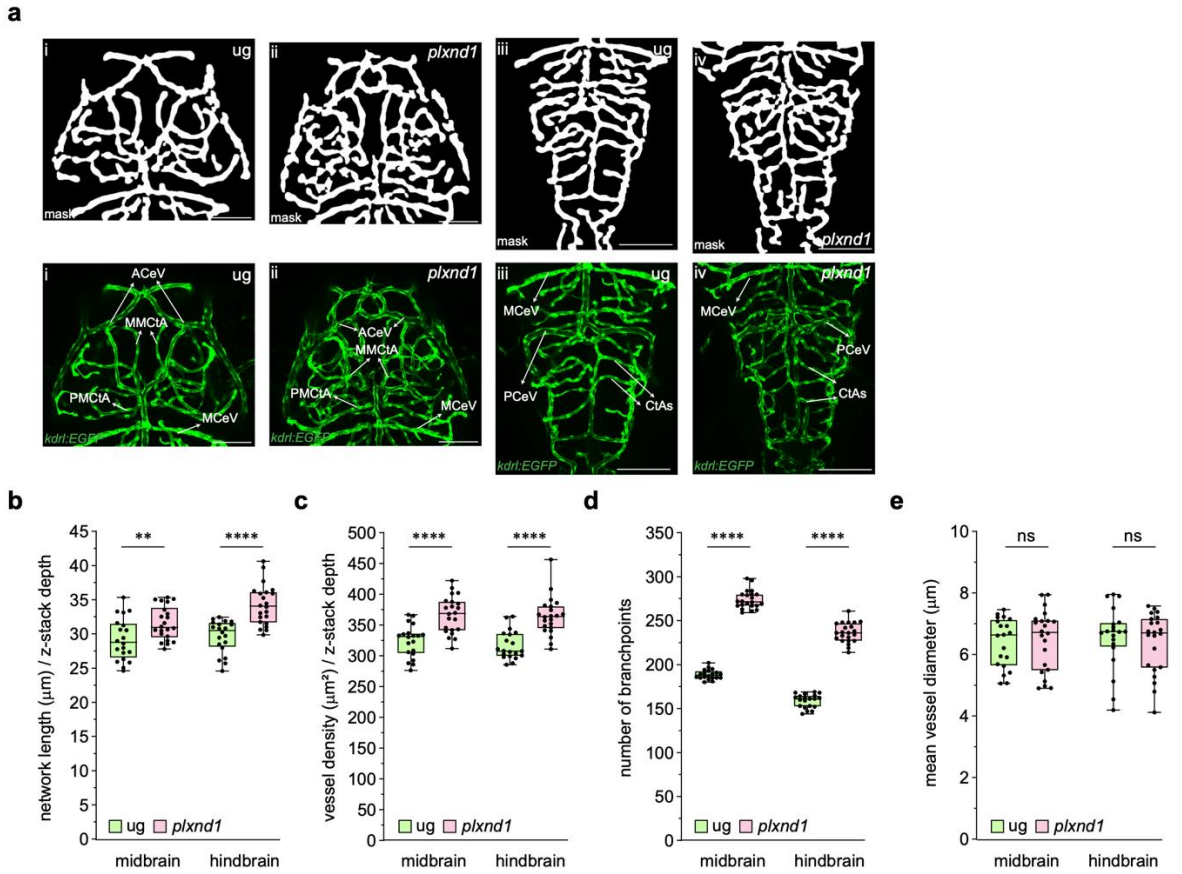

Fig. S7. VISTA-Z detects midbrain and hindbrain ectopic angiogenesis in *plxnd1* crispants. a) Enlarged views of the brain vasculature from (**Fig. 6a**) showing midbrain (i and ii) and hindbrain (iii and iv) regions from universal guide (ug) injected controls (left) and *plxnd1* crispants (right) at 3 dpf. Vessel segmentation masks (top) and confocal images (bottom). **b - e**) Quantification of vascular metrics in midbrain and hindbrain segments, including normalised network length (**b**, p = 0.0089 (midbrain) and p ≤ 0.0001 (hindbrain)), vessel density (**c**, p ≤ 0.0001 (midbrain) and p ≤ 0.0001 (hindbrain)), number of branchpoints (**d**, p ≤ 0.0001 (midbrain) and p ≤ 0.0001 (hindbrain)), and vessel diameter (**e**, ns = 0.7936 (midbrain) and ns = 0.6859 (hindbrain)). All panels represent n = 20 wild type and n = 23 mutant embryos. Embryos were obtained from two independent breeding pairs. Statistical significance was assessed using unpaired Student's t-test for all panels, except for panels (**b** and **c**: hindbrain and **e**), which used Mann–Whitney U test. ACeV: anterior cerebral vein, CtAs: central arteries, MCeV: middle cerebral vein, PCeV: posterior cerebral vein and PMCtA and MMCtA: posterior and middle mesencephalic central arteries. Scale bars = 100μm.

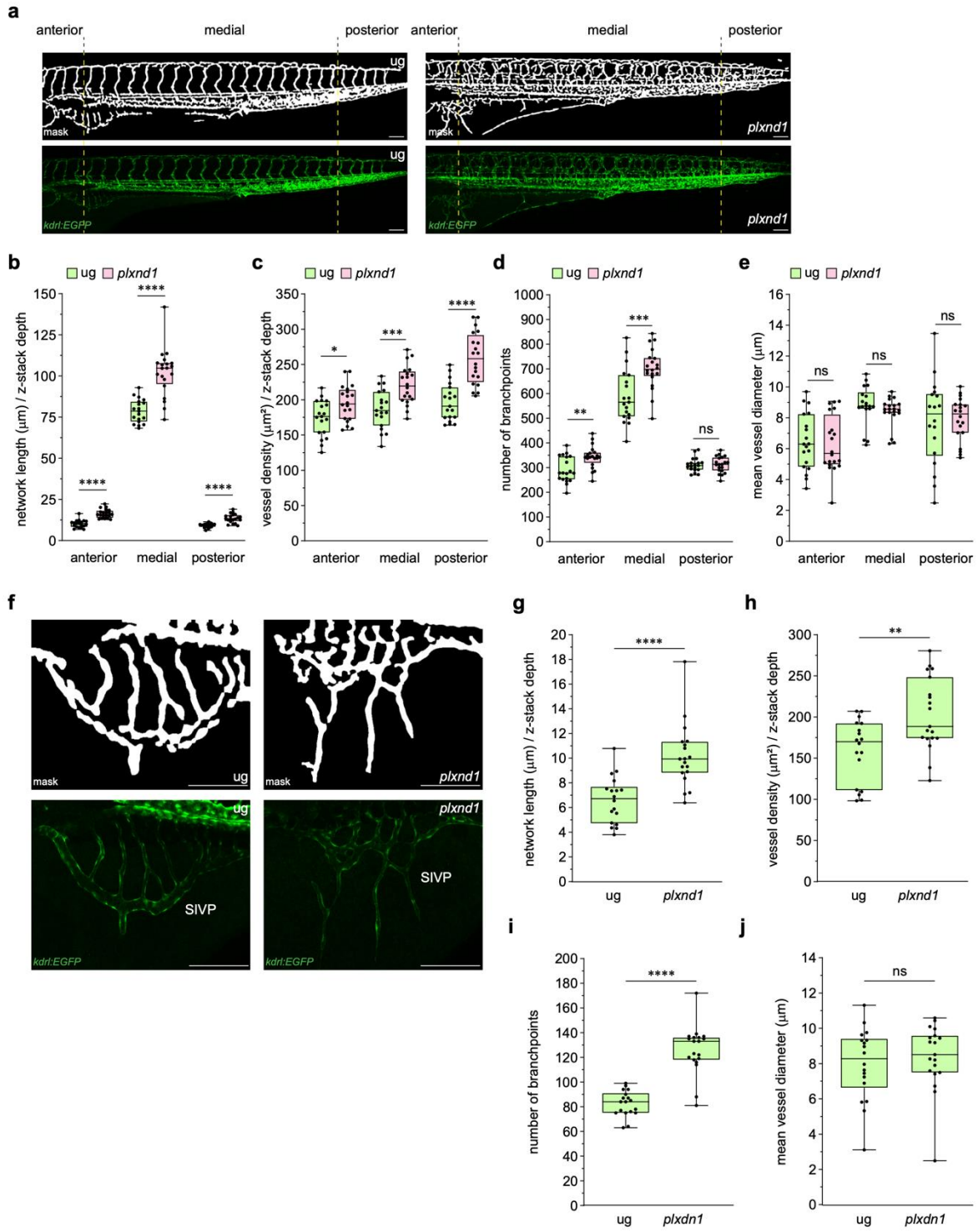

Fig. S8. VISTA-Z reveals widespread trunk hyper-vascularisation in *plxnd1* crispants. a) Vessel segmentation masks (top) and confocal images (bottom) of the trunk vasculature from universal guide (ug) injected controls (first and second) and *plxnd1* crispants (third and fourth) at 3 dpf. Regiones were defined as: anterior (ISVs 1-4), medial (ISVs 5-25), and posterior (ISVs 26-30). **b - e**) Quantification of vascular metrics in anterior, medial and posterior segments, including normalised network length (**b**, $p \leq 0.0001$ (anterior), $p \leq 0.0001$ (medial) and $p \leq 0.0001$ (posterior)), vessel density (**c**, $p = 0.0128$ (anterior), $p = 0.0004$ (medial) and $p \leq 0.0001$ (posterior)), number of branchpoints (**d**, $p = 0.0025$ (anterior), $p = 0.0009$ (medial) and ns = 0.9038 (posterior)), and vessel diameter (**e**, ns = 0.8350 (anterior), ns =

0.099 (medial) and ns = 0.8263 (posterior)). **f**) Enlarged views of the SIVP from (**Fig. 6f**) from control-injected embryos (left) and *plxnd1* crispants (right). Vessel segmentation masks (top) and confocal images (bottom). **g - j**) Quantification of SIVP metrics, including normalised network length (**g**, $p \leq 0.0001$), vessel density (**h**, $p = 0.0055$), number of branchpoints (**i**, $p \leq 0.0001$), and vessel diameter (**j**, ns = 0.4797). Panels represent n = 19 control-injected and n = 20 *plxnd1* crispants (**b - e**) or n = 18 control-injected and n = 19 *plxnd1* crispants (**g - j**). Embryos were obtained from two independent breeding pairs. Statistical significance was assessed using unpaired Student's t-test for all panels, except for panels (**b**: medial and **e**: anterior and medial, and **g - j**), which used Mann–Whitney U test. ISV: intersegmental vessel and SIVP: sub-intestinal vein plexus. Scale bars = 100μm.